# Distance Dependence of the Charge Transfer Rate for Peptide Nucleic Acid Monolayers

**ARTICLE** *in* THE JOURNAL OF PHYSICAL CHEMISTRY B · SEPTEMBER 2009

Impact Factor: 3.3 · DOI: 10.1021/jp906910h · Source: PubMed

# Distance Dependence of the Charge Transfer Rate for Peptide Nucleic Acid Monolayers†

**Amit Paul,‡ Richard M. Watson,§ Emil Wierzbinski,‡ Kathryn L. Davis,‡ Allen Sha,§ Catalina Achim,*,§ and David H. Waldeck*,‡**

*Department of Chemistry, University of Pittsburgh, Pennsylvania 15260, and Department of Chemistry, Carnegie Mellon University, Pittsburgh, Pennsylvania 15213*

*Received: July 21, 2009; Revised Manuscript Received: July 29, 2009*

Charge transfer studies have been performed for self-assembled monolayers of single-stranded and double-stranded peptide nucleic acids (PNAs) having a C-terminus cysteine and an N-terminus ferrocene group as a redox reporter. The decay of the charge transfer rate with distance was strong for short single-stranded PNA molecules and weak for long single-stranded and double-stranded PNAs. Possible mechanisms for this "softening" of the distance dependence are discussed. The nature of the mechanism change can be explained by a transition of the charge transport mechanism from superexchange-mediated tunneling for short PNAs to a "hopping" mechanism for long PNAs.

## Introduction

The mechanism of charge transfer through deoxyribonucleic acid (DNA) has been a highly debated topic in the scientific community during the past 15 years.[1−19] Questions about whether DNA is a molecular wire, and whether the charge transport takes place through the "$\pi$-stack" or not, have been addressed by a number of groups.[2,4−8,13,15−17,20,21] The debate surrounding the charge transfer properties of DNA has also sparked interest in the nature of charge transfer through self-assembled monolayers (SAMs)[22,23] of nucleic acids and their potential applications in the field of molecular electronics.[24] We studied charge transfer in peptide nucleic acid, PNA, as an alternative to DNA, in an effort to better elucidate the important factors that control charge transfer through nucleic acids.

Charge transfer through double-stranded (ds) DNA in solution has been extensively studied by several research groups. Fewer studies have focused on charge transfer through single-stranded (ss) DNA, presumably because the flexible ss DNA can adopt conformations in which the charge donor and acceptor are close to each other even if they are separated by several nucleobase units. This property makes it difficult to distinguish between transport along the chain and transfer limited by conformationally driven association of guanines.[25,26] For example, Schuster and co-workers have shown that holes injected into duplex DNA can migrate into ss DNA overhangs, and suggested that the radical cation transport proceeds between G nucleobases by direct contact in GG mispairs.[26] Melvin et al. have used flash photolysis to initiate and study hole migration in ss DNA and found that the nature of the base pairs between G sites affects the transport.[27] Most of the studies indicated that hole transport along ss DNA is considerably slower than in ds DNA.

Compared to charge transfer of DNA in solution, fewer electrochemical studies have been dedicated to the characterization of charge transfer through self-assembled monolayers (SAMs) of DNA. Barton and co-workers have studied SAMs of DNA to which small molecules have been attached by covalent or noncovalent bonds using electrochemical methods.[28−31] Their work showed that charge transfer takes place through the base stack and is sensitive to structural perturbations of the nucleobase stacking. Kraatz and co-workers have studied charge transfer through SAMs of ferrocene-containing DNA and reported a charge transfer rate constant of 12 $s^{-1}$ for ss DNA (20 bases) and 25−115 $s^{-1}$ for ds DNA (20 base pairs).[32,33] Anne and co-workers have also explored electron transfer between a redox reporter (ferrocene) attached to ss DNA and electrodes.[34,35] In those assemblies, the surface coverage of DNA was low (ca. 5 pmol/$cm^2$) and the electron transfer was found to be conformationally gated by bending of the DNA strand toward the electrode surface.

To date, single molecule conductance measurements have been performed on relatively short DNA oligonucleotides. While some of the variability of the experimental conductance values obtained in these studies was caused by differences in experimental conditions and difficulties in forming reliable metal−molecule contacts, a clear dependence of the electrical conductivity of DNA on the nucleobase sequence has been observed by break junction,[36,37] scanning tunneling spectroscopy techniques,[38,39] current sensing atomic force microscopy,[40,41] and carbon nanotube nanogap devices.[42] Naaman,[40] Tao,[36] Nichols,[38] and their co-workers have independently demonstrated that the presence of guanines in ds DNA enhances the single molecule conductance of DNA. Studies on ds DNA containing one mismatch showed that their conductance is 5−300 times lower than that of fully complementary sequences.[37,39,42] Although most studies have focused on DNA duplexes, single molecule measurements have shown that charge transfer occurs through ss DNA oligonucleotides and that it depends on the sequence of the ss DNA.[38,42] This finding indicates that the nucleobases participate in the charge transfer through ss DNA.[38]

The discussion of the mechanism of charge transport through DNA has been based primarily on studies of ds DNA in solution. For example, Giese and co-workers have studied hole transfer between guanines (G) in ds DNA by varying the number of adenine−thymine (AT) base pairs situated between the G bases.[4,6,7,13] They have shown that, if the number of intervening AT base pairs is smaller than three, then the AT base pairs act as a superexchange bridge, which is not oxidized during single step hole transfer. Thus, at short distance, charge transfer follows

† Part of the "Michael R. Wasielewski Festschrift".
‡ University of Pittsburgh.
§ Carnegie Mellon University.

10.1021/jp906910h 
Published on Web 08/19/2009

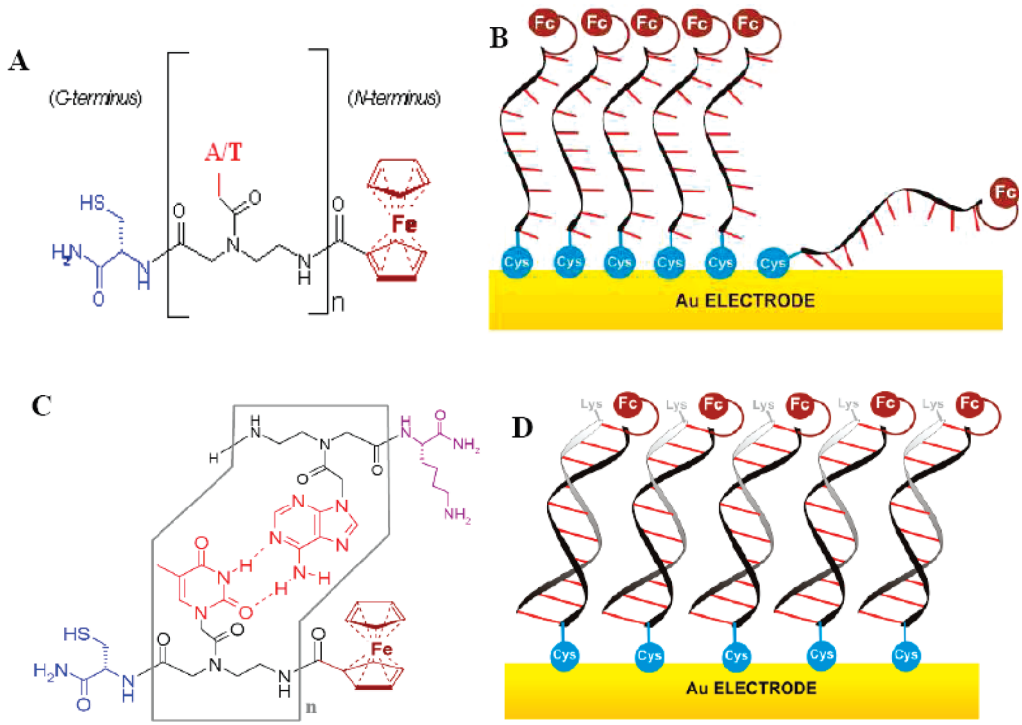


**Figure 1.** (A) Chemical structure of ss PNA that has a C-terminus cysteine and an N-terminus ferrocene. In our studies, the nucleobase is adenine or thymine and $n = 3-10$. (B) Schematic representation of ss PNA molecules self-assembled on a gold surface. The blue circle represents cysteine, the black curl represents the PNA backbone, the red lines represent A or T nucleobases, and the light brown circle represents ferrocene. (C) Chemical structure of ds-$(AT)_n$-PNA that has a C-terminus cysteine and an N-terminus ferrocene, where $n = 7-10, 15$. (D) Schematic representation of ds PNA molecules self-assembled on a gold surface, in which the blue circle represents cysteine, the gray curl represents the PNA backbone, the red lines represent the AT nucleobase pair, and the brown circle represents ferrocene.

a superexchange mechanism,[43−53] in which the charge tunnels from the first site to the last site by a single coherent jump. If this mechanism is active, the charge transfer rate decays exponentially with the distance, and it is not effective beyond a few nanometers. Giese found that, when the number of AT base pairs is larger than three, endothermic oxidation of adenine occurs and the hole migrates by hopping through the adenines until it reaches a guanine base (see ref 6 and references therein). Thus, for longer distance transport, the charge "hops" through the intervening base pairs in DNA. Wasielewski and co-workers studied the dynamics of hole transport in DNA as well.[16,21] Their studies showed that the hole transport depends on the sequence and length of DNA that separates the primary and secondary donors and on the location of the donors. They have observed that (1) the rate constant increases as the hole transport goes from being isoergic to exergonic, (2) the hole transport rates are very large ($\sim 10^7$ $s^{-1}$), and (3) the charge can migrate through the bridging sites before chemical reactions can occur at the oxidized base pairs.[16,21]

The detailed mechanism of long distance transport remains under discussion, and a number of different models have been proposed. According to the incoherent multistep hopping mechanism,[3,4,6,7,9,10,12,13,16,19,54] the charge diffuses from the donor to the acceptor and is localized on individual "hole resting sites", modeled as a one-dimensional random walk with an absorbing sink at the acceptor. Schuster and co-workers proposed a "polaron-like" hopping mechanism,[2,8,17] in which local energy-lowering structural distortions generate a self-trapped state of finite extent that migrates from one location to another by thermal (phonon) activation. So far, most of the studies of charge transfer in ds DNA showed that the G and A nucleobases act as hole resting sites because their oxidation potentials are lower than those of T and C.

An alternative to DNA for realizing nucleic acid SAMs is peptide nucleic acid (PNA). PNA is a synthetic analogue of DNA that commonly has a neutral and achiral backbone composed of *N*-aminoethylglycine units, in contrast to the negatively charged and chiral backbone of DNA (Figure 1A).[55,56] The neutral backbone of PNA makes it a promising candidate for monolayer self-assembly. PNA forms duplexes with complementary PNA or DNA strands by Watson−Crick base pairing. PNA·PNA duplexes adopt a helical structure termed the P type, which has a large pitch with 18 bases/turn, a diameter of 28 Å, and a 3.2−3.4 Å rise/base pair.[57−60] A preferred handedness can be induced in PNA duplexes by chiral amino acids situated at the C-terminus of the PNA.[61] Moreover, ligand-modified PNA can be used as a scaffold for the incorporation of transition metal ions at specific positions within the duplex.[62−64] In voltammetry studies of ss PNA films, we have observed direct electron tunneling through high coverage (ca. 100 pmol/$cm^2$) SAMs of PNAs of up to seven nucleobases and demonstrated the dependence of the rate constant on the nucleobase identity.[65,66] These findings indicated that charge transfer in these PNA SAMs takes place by a superexchange-mediated tunneling mechanism, which is very different from the conformational gating mechanism identified by Anne et al. for SAMs of DNA.[41,42]

In this work, PNA SAMs were grown on gold electrodes. PNA with a ferrocene redox probe covalently attached at the N-terminus was immobilized on a gold surface through a cysteine group situated at the C-terminus (Figure 1B). This study focused on the charge transfer of three different types of PNAs: (i) ss thymine PNA Cys-$T_n$-Fc, (ii) ss adenine PNA Cys-$A_n$-Fc, and (iii) ds adenine−thymine PNA Cys-$(AT)_n$-Fc, where both the cysteine and ferrocene were attached to the thymine strand. Cyclic voltammetry (CV) was used to measure the charge transfer rate between the gold electrode and the ferrocene redox

reporter. Ellipsometry was used to measure the film thickness.[67,68] For short ss PNA molecules, the charge transfer rate fell rapidly with increasing chain length, which is consistent with a superexchange-mediated tunneling mechanism. However, for long PNAs, the charge transfer rate had a weaker distance dependence and it correlated with the oxidation potential of the nucleobases, suggesting a hopping mechanism for the charge transfer.

## Experimental Section

**PNA Synthesis.** PNA oligomers were synthesized by solid phase peptide synthesis using the Boc protection strategy.[69−71] MBHA resin (Peptides International, Louisville, KY) with a loading of 0.18 mEq/g was down-loaded[55] using Boc-L-Cys-(4-MeOBzl)-OH or Boc-L-Lys-(4-MeOBzl)-OH (NovaBiochem/Merck Biosciences, Switzerland) to an estimated loading of 0.04−0.06 mEq/g. Boc-T-OH or Boc-A-OH PNA monomers (Applied Biosystems, Foster City, CA) were coupled using 1*H*-benzotriazolium 1-[*bis*(dimethylamino)methylene]-5-chlorohexafluorophosphate (1),3-oxide (HCTU) (Peptides International) to create PNAs containing 3−10, or 15 bases. Finally, ferrocenecarboxylic acid (Aldrich) was coupled to the N-terminus. This coupling of the ferrocene was repeated twice. The PNA oligomers were cleaved from the resin using trifluoroacetic acid and trifluoromethanesulfonic acid, precipitated in ethyl ether, and dried under nitrogen. The solid products were dissolved in 15% acetonitrile aqueous solution and purified by reverse-phase HPLC using a solvent gradient from 15 to 35% acetonitrile in water over 40 min on an HPLC system with a Waters Delta 600 pump and a 2996 photodiode array detector (Milford, MA). PNA oligomers were characterized by MALDI-ToF mass spectrometry on an Applied Biosystems Voyager-DE STR Workstation.

PNA solutions were prepared in deionized water, and the PNA concentrations were determined by UV−vis spectrophotometry assuming $\varepsilon_{260} = 8600$ and 13700 $cm^{-1}$ $M^{-1}$ for each T and A monomer, respectively.[71] PNA solutions for electrode incubation were typically 20 $\mu$M ss PNA in a 1:1 v/v mixture of 10 mM pH 7.0 sodium phosphate buffer and acetonitrile. PNA duplexes were prepared by heating solutions that were 20 $\mu$M Cys-$T_n$-Fc and 20 $\mu$M Lys-$A_n$ PNA at 95 °C for 5 min and then slowly cooling them (~1 h) to room temperature. SAMs of ds PNA were made using PNA oligomers that have at least seven A or T nucleobases, in order to ensure that the room temperature SAMs formed from solutions of the two complementary strands contain a majority of ds-$(AT)_n$ PNA.

**Electrode Preparation.** A gold wire (0.5 mm diameter, 99.999%, Alfa Aesar, MA) was cleaned by refluxing in 70% nitric acid at 130 °C for 2 h and then washed with deionized water (>18 MΩ·cm). The wire was sealed in a soft-glass capillary tube with the tip exposed. The tip of the gold wire was heated to form a ball. The gold ball was reheated in a flame until glowing, then slowly cooled down, and finally quenched in deionized water. This annealing process was repeated more than 15 times until a smooth ball electrode was obtained. The area of the electrode was determined electrochemically[72] and found to be ~0.1 $cm^2$.

**Self Assembled Monolayer (SAM) Preparation.** Self-assembled monolayers of ss PNA and ds PNA molecules were prepared by incubating gold ball electrodes in 1 mL of a 20 $\mu$M PNA solution for 28−40 h at 35−40 °C and at 27 °C, respectively. After incubation, the gold electrodes were washed with deionized water and directly used in the electrochemical studies.

**Mixed Duplex PNA/*n*-Octadecanethiol Self-Assembled Monolayer Preparation.** The mixed ds PNA/*n*-octadecanethiol SAMs were prepared by a two-step process. Gold electrodes were covered by a submonolayer of ds PNA, which was formed during overnight incubation of the electrodes in a 5 $\mu$M PNA solution in acetonitrile/water/ethanol 1:1:2 (v/v/v) at 27 °C. To complete the monolayer with a octadecanethiol matrix, we adopted the method of the preparation of electrooxidation of octadecylthiosulfates proposed by Lee et al.[73] The details of the preparation of the mixed monolayer are provided in the Supporting Information.

**Electrochemical Measurements.** Cyclic voltammetry was carried out on a CH Instruments 618B Electrochemical Analyzer (Austin, TX). The three-electrode electrochemical cell consisted of an Ag/AgCl (3 M/1 M KCl) reference electrode, a platinum wire as the counter electrode, and a SAM coated gold ball electrode as the working electrode. All experiments were performed in 1.0 M $NaClO_4$ (pH 7−8) aqueous electrolyte solution at room temperature. The uncompensated solution resistance was measured by AC impedance and found to be less than 5 Ω, so that the iR drop was not important for these measurements. The coverage of the PNA−ferrocene SAM was calculated by integrating the charge under the voltammetric peaks.

**Ellipsometry.** The molecules were self-assembled to form a monolayer film on evaporated gold slides (EMF Corp, Ithaca, NY). The Au slides were 0.7 in. × 0.3 in. × 0.062 in. in size and consisted of about 100 nm Au over a 50 nm thick Ti binder layer on float glass. The gold slides were cleaned by immersion in "piranha" solution (1:3 $H_2O_2$ and 98% $H_2SO_4$) **(Caution! The piranha solution is a very strong oxidizing agent and extremely dangerous. Eye protection and gloves should be used during handling.)** for 2 min and then rinsed by a large amount of deionized water, followed by ethanol. The slides were subsequently dried under nitrogen. For PNA SAM formation, the Au slides were incubated according to the conditions specified earlier. After incubation, these SAM coated gold slides were rinsed vigorously with ethanol and water and dried under nitrogen. The thickness was measured using a Gaertner L-117 Null ellipsometer.

**PNA Duplexes versus Triplexes.** PNA sequences containing only adenine and thymine were selected for this study because of their high oxidation potentials, which allows us to probe the charge transfer properties of the SAMs without complications arising from oxidizing guanine. Given that PNA triplexes are known to form in solutions of adenine and PNA,[74] we have considered whether triplexes form in the SAM when preparing them from solutions containing Cys-$T_n$-Fc and Lys-$A_n$. By intentionally using solution conditions that favor triplex formation, it was possible to create films with very slow electrochemical rates, a finding that is consistent with earlier reports for electron transfer through triplexes.[75,76] The supporting material describes these control studies and shows that duplexes are formed under the deposition conditions used in this study.

## Results

**Thickness and Voltammetric Studies.** Ellipsometry was used to determine the film thickness by measuring the change in light polarization upon reflection by the SAM coated gold surface. As discussed previously,[66] a refractive index of 1.6 was used for the calculation of the thickness of the SAM. The measured and estimated PNA SAM thicknesses are reported in Tables 1 and 2. The lengths of the molecules have been estimated by adding characteristic lengths for the cysteine (4

**TABLE 1: Thicknesses of ss PNA SAMs and Estimated Length of ss PNA**

| PNA | ellipsometric thickness (nm) | calculated length (nm) | PNA | ellipsometric thickness (nm) | calculated length (nm) |
|---|---|---|---|---|---|
| Cys-$T_3$-Fc | 1.4 ± 0.1 | 1.95 | | | |
| Cys-$T_4$-Fc | 1.4 ± 0.1 | 2.30 | Cys-$A_4$-Fc | 1.6 ± 0.2 | 2.30 |
| Cys-$T_5$-Fc | 1.3 ± 0.1 | 2.65 | | | |
| Cys-$T_6$-Fc | 2.1 ± 0.1 | 3.00 | Cys-$A_6$-Fc | 1.8 ± 0.1 | 3.00 |
| Cys-$T_7$-Fc | 2.3 ± 0.1 | 3.35 | Cys-$A_7$-Fc | 2.2 ± 0.2 | 3.35 |
| Cys-$T_8$-Fc | 2.6 ± 0.1 | 3.70 | Cys-$A_8$-Fc | 2.5 ± 0.1 | 3.70 |
| Cys-$T_9$-Fc | 3.1 ± 0.1 | 4.05 | | | |
| Cys-$T_{10}$-Fc | 3.0 ± 0.2 | 4.40 | Cys-$A_{10}$-Fc | 3.2 ± 0.2 | 4.40 |

**TABLE 2: Thicknesses for ds PNA SAMs and Estimated Length of ds PNA**

| duplex | ellipsometric thickness (nm) | calculated length (nm) |
|---|---|---|
| Cys-$(AT)_7$-Fc | 2.5 ± 0.2 | 3.28 |
| Cys-$(AT)_8$-Fc | 3.2 ± 0.2 | 3.62 |
| Cys-$(AT)_9$-Fc | 3.5 ± 0.1 | 3.96 |
| Cys-$(AT)_{10}$-Fc | 3.6 ± 0.1 | 4.30 |
| Cys-$(AT)_{15}$-Fc | 5.1 ± 0.2 | 6.00 |

Å), the ferrocene (5 Å), and each PNA base (3.5 Å for ss PNA and 3.4 Å for ds PNA).[57−60,77]

The ellipsometric thicknesses of the ss PNA SAMs were considerably smaller than the calculated lengths of the molecules. In order to understand the ellipsometry results, the PNA SAMs can be modeled in two different ways.[66] In the first case, the PNA SAM was modeled as compact and formed from PNA molecules tilted on the surface at some angle from the surface normal. In the second case, the PNA SAM was modeled by a mixture of a certain population of "lying-down" molecules and a second population of "standing-up" molecules. In previous work,[66] on the basis of a consistent set of ellipsometry, voltammetry, and AFM measurements, we showed that the second model is more appropriate for ss PNA SAMs. For SAMs formed from Cys-$T_3$-Fc to Cys-$T_7$-Fc molecules, the percentage of "lying-down" molecules ranged from 9 to 19%.[66] For the new monolayer assemblies reported here, the ellipsometry measurements give percentages of "lying-down" molecules that are within a similar range, i.e., 7.1 ± 0.7% for Cys-$T_8$-Fc, 5.1 ± 0.5% for Cys-$T_9$-Fc, 6.2 ± 0.9% for Cys-$T_{10}$-Fc, 13 ± 4% for Cys-$A_4$-Fc, 12 ± 1% for Cys-$A_6$-Fc, 9 ± 2% for Cys-$A_7$-Fc, 7.8 ± 0.7% for Cys-$A_8$-Fc, and 5 ± 1% for Cys-$A_{10}$-Fc.

The voltammetry of the ss PNA SAMs indicated the presence of two types of ferrocene molecules with different charge transfer rates. One species had a fast rate, which was attributed to through space charge transfer between the redox probe and the gold electrode for the molecules that are "lying down" on the gold surface. The second species had a slower charge transfer rate, which was attributed to the response of "standing-up" molecules in which charge transfer occurs through the PNA molecule. This feature of the SAMs was characterized and discussed at length in an earlier report.[66] To study the "standing-up" population of the PNAs, the redox probe of the "lying-down" molecules was electrochemically destroyed, using a previously described protocol.[66] In this method, the ferrocenium of the "lying-down" phase is preferentially reacted with $Cl^-$,[66,78] and becomes electrochemically silent. Subsequently, the charge transfer rates for "standing-up" molecules can be measured in $NaClO_4$ solution, in which the ferrocenium is stable (see ref 66 for details on this procedure).

The ellipsometric thickness of ds PNA SAMs (Table 2) was higher than that of the corresponding ss PNA SAMs, which indicates that the ds PNA SAMs were more uniform and compact than ss PNA SAMs. There is still a difference between the measured thickness of the SAM and the calculated length of a ds PNA molecule, which could arise from tilting of the molecules with respect to the surface normal, similar to what has been observed for close-packed alkanethiol SAMs, or from the coexistence of a mixture of "standing-up" and "lying-down" molecules. Unfortunately, ellipsometric thickness determinations are not so useful for distinguishing the "standing-up" from the "lying-down" phase of the seven-base-pair PNA duplexes because their width (2.8 nm)[57−59] and length (3.3 nm) are comparable.

The voltammetry measurements suggest that the ds PNA SAMs are more homogeneous than the ss PNA SAMs, but in about 75% of the voltammetry experiments on ds PNA SAMs, a small percentage of molecules (≤3%) with a fast charge transfer rate were observed. In the other 25% of the samples, voltammetry experiments showed no clear evidence of a fast charge transfer species. The species with a fast charge transfer rate, observed in some of the ds PNA SAMs, could be "lying-down" molecules of ds PNA or ss PNA. Regardless of its chemical nature, in each case in which the voltammetry experiments showed the presence of a faster species, this species has been selectively destroyed using the protocol previously developed for ss PNA SAMs (see above).[66]

**Rate Constant Determination for Different PNA SAMs.** Cyclic voltammetry was used to measure the charge transfer rate through the "standing-up" population of PNA SAMs. Representative cyclic voltammograms collected at 20, 30, and 40 mV/s for Cys-$(AT)_7$-Fc are shown in Figure 2A. These voltammograms show that, as the scan rate is increased, the voltammetric peak shifts, indicating that the charge transfer event becomes slow with respect to the scan rate. Figure 2B is a plot of the oxidation peak potential versus the scan rate. The data have been fit using Marcus theory, in which the standard electrochemical rate constant $k^0$ was used as an adjustable parameter and assuming that the reorganization energy for ferrocene is 0.8 eV.[66,79] We note that a change in this value of the reorganization energy of up to 25% does not affect the quality of the fitting. The voltammograms and fitting curves of other PNA SAMs are provided in the Supporting Information (Figures S5−S25).

The charge transfer rate constants $k^0$ for ss-$T_n$-PNA and ss-$A_n$-PNA molecules are reported in Table 3, and the logarithm of the charge transfer rate constant is plotted versus the number of nucleobases in Figure 3. For ss PNA with more than seven nucleobases, the dependence of the charge transfer rate constant on the distance is weak and the $k^0$ value of ss-$A_n$-PNA is consistently 6−8 times higher than that of ss-$T_n$-PNA. Assuming a tunneling model for charge transfer in the short ss PNAs (≤7 nucleobases), one can fit the data shown in Figure 3 with a tunneling decay parameter of 3.0 ± 0.1 per nucleobase and 2.7 ± 0.2 per nucleobase for ss-T and ss-A, respectively. If one further assumes a characteristic length of 3.5 Å per nucleobase,[77] the corresponding $\beta$ values for these PNAs are 0.86 ± 0.04 $Å^{-1}$ for the ss-$T_n$-PNA[66] and 0.76 ± 0.06 $Å^{-1}$ for the ss-$A_n$-PNA. The difference in the distance dependence of the rate constant between short and long ss PNAs indicates that the charge transfer proceeds by different mechanisms in these two types of PNAs.

Extrapolation of the electron transfer rate constant to zero distance, i.e., to contact between ferrocene and the electrode, leads to a value for the maximum electron transfer rate constant of $5.8 \times 10^8$ $s^{-1}$ from the ss-T-oligomer data and $2.8 \times 10^8$ $s^{-1}$ from the ss-A-oligomer data. These values are in reasonable

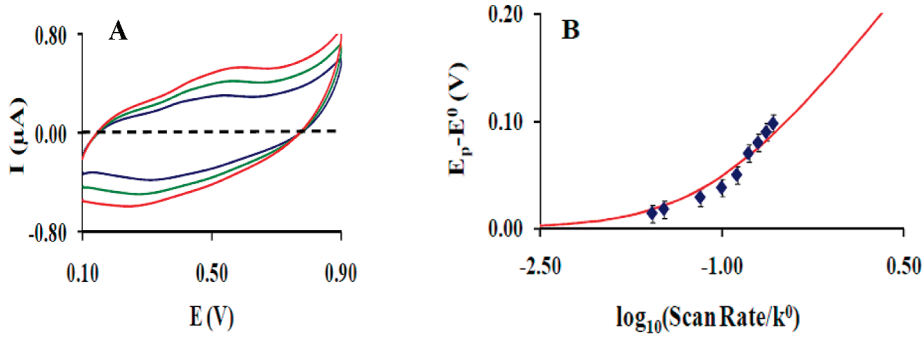


**Figure 2.** (A) Cyclic voltammograms are shown for Cys-$(AT)_7$-Fc SAM at scan rates 20 mV/s (blue), 30 mV/s (green), and 40 mV/s (red). (B) A fitting curve is plotted for the determination of the charge transfer rate of Cys-$(AT)_7$-Fc SAM. The diamond symbols represent the experimentally determined points, and the solid line represents the best fit theoretical curve. Error bars represent the error in peak position determination.

**TABLE 3: $k^0$ for the "Standing-up" Population of ss PNA SAMs**

| oligomer | $k^0$ ($s^{-1}$) | oligomer | $k^0$ ($s^{-1}$) |
|---|---|---|---|
| Cys-$T_3$-Fc | 2000 ± 200 | | |
| Cys-$T_4$-Fc | 200 ± 20 | Cys-$A_4$-Fc | 275 ± 18 |
| Cys-$T_5$-Fc | 3.0 ± 0.5 | | |
| Cys-$T_6$-Fc | 0.14 ± 0.03 | Cys-$A_6$-Fc | 1.2 ± 0.1 |
| Cys-$T_7$-Fc | 0.018 ± 0.002 | Cys-$A_7$-Fc | 0.12 ± 0.03 |
| Cys-$T_8$-Fc | 0.014 ± 0.004 | Cys-$A_8$-Fc | 0.10 ± 0.01 |
| Cys-$T_9$-Fc | 0.008 ± 0.002 | | |
| Cys-$T_{10}$-Fc | 0.007 ± 0.003 | Cys-$A_{10}$-Fc | 0.04 ± 0.01 |

agreement with that reported by Smalley et al.[80] for ferrocene terminated alkanethiol ($6 \times 10^8$ $s^{-1}$).

The rate constant $k^0$ for ds-$(AT)_n$-PNA has been measured by voltammetry in pure SAMs and in mixed *n*-octadecanethiol/ds-$(AT)_n$-PNA SAMs (see Table 4). The charge transfer rate

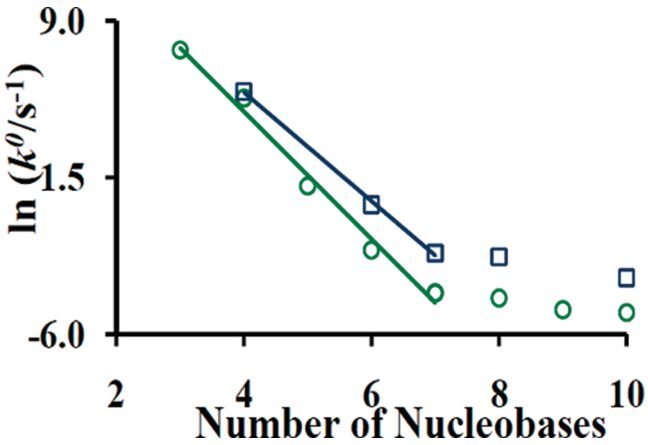


**Figure 3.** Charge transfer rate constant $k^0$ of PNA molecules as a function of the number of nucleobases in the PNA. Green circle and blue square symbols represent ss-$T_n$-PNA and ss-$A_n$-PNA, respectively (error bars are smaller than symbols). The solid lines represent the best fit to tunneling decay for PNA molecules with $n \leq 7$.

**TABLE 4: $k^0$ for Pure ds-$(AT)_n$ and Mixed Octadecanethiol/ds-$(AT)_n$ PNA SAMs**

| duplex | pure SAM $k^0$ ($s^{-1}$) | pure SAM coverage (pmol/$cm^2$) | mixed SAM $k^0$ ($s^{-1}$) |
|---|---|---|---|
| Cys-$(AT)_7$-Fc | 0.25 ± 0.05 | 109 ± 38 | 0.80 ± 0.15 |
| Cys-$(AT)_8$-Fc | 0.24 ± 0.08 | 66 ± 36 | 0.70 ± 0.10 |
| Cys-$(AT)_9$-Fc | 0.14 ± 0.07 | 90 ± 23 | 0.21 ± 0.04 |
| Cys-$(AT)_{10}$-Fc | 0.09 ± 0.02 | 63 ± 9 | 0.09 ± 0.02 |
| Cys-$(AT)_{15}$-Fc | 0.038 ± 0.005 | 87 ± 30 | *a* |

[a] $k^0$ could not be determined for the 15-mer in mixed SAM because of low signal levels.

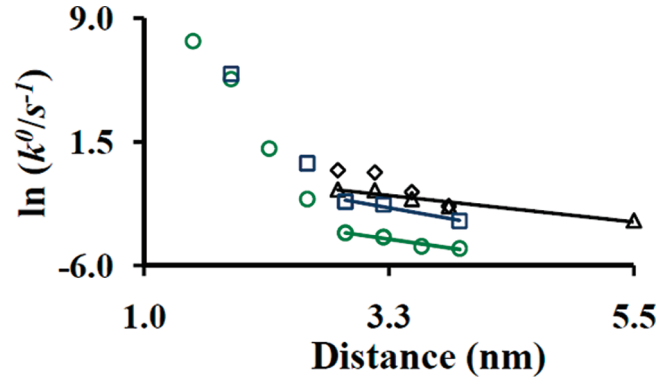


**Figure 4.** Charge transfer rate constants of PNA molecules plotted as a function of the distance between the Au electrode and the ferrocene. Green circle, blue square, and black triangle symbols represent ss-$T_n$-PNA, ss-$A_n$-PNA, and ds-$(AT)_n$-PNA, respectively. Black diamond symbols represent the charge transfer rate constants of a mixed octadecanethiol/ds-$(AT)_n$-PNA monolayer. The solid lines represent the best fit line to the measured decay rate constants at long chain length, corresponding to $\beta = 0.1 \pm 0.1$ $Å^{-1}$ for ss-$T_n$-PNA, $\beta = 0.1 \pm 0.1$ $Å^{-1}$ for ss-$A_n$-PNA, and $\beta = 0.07 \pm 0.03$ $Å^{-1}$ for ds-$(AT)_n$-PNA.[1]

constants in both types of SAMs are similar and show a weak decay with the distance; we note that some deviation between the two data sets occurs at shorter lengths and may reflect a higher electronic coupling for the mixed films. The origin of this difference requires further investigation; however, it is small with respect to the large dynamic range of rate constants reported in Figure 4. The charge transfer rates of the ds-$(AT)_n$-PNA were consistently 14−15 times higher than the corresponding ss-$T_n$-PNA and were 2 times higher than the ss-$A_n$-PNA when $n \geq 7$.

For $n \geq 7$, a weak distance dependence is evident for all of the PNAs (Figure 4). The ds-$(AT)_n$-PNA shows a weak distance dependence of $\beta = 0.07 \pm 0.03$ $Å^{-1}$. This value is in excellent agreement with the 0.07 $Å^{-1}$ value reported by Giese[20] for hopping transport between G sites on duplex DNA. Although the best fit $\beta$ parameter for the ss PNA (ca. 0.1 $Å^{-1}$, see Figure 4) is somewhat larger than that reported for the duplex PNA, those data have a significant uncertainty because of the limited range of chain lengths that could be studied ($n = 7-10$). Hence, the small change of rate constant with distance may not be significant in these cases.

## Discussion

Our results indicate a change in the charge transfer mechanism with film thickness. For short distances between the electrode and the ferrocene (<7 nucleotides), the charge transfer rate constant decreases exponentially with distance, and the falloff is consistent with a coherent superexchange-mediated tunneling

mechanism, as discussed previously for other types of SAMs, most notably alkanethiols.[80−84] At larger film thicknesses (>7 nucleotides), the charge transfer rate constant has a weaker distance dependence. A number of different models, involving incoherent transport, have been used to explain such findings. A model for the charge transfer rate should account for the difference between the distance dependence of the rate constants in short and long PNAs and for the difference between rate constants of PNAs made of different nucleobases, e.g., A or T. The charge transfer rate constant of ss-$T_n$-PNA was consistently 6−8 times slower than that of ss-$A_n$-PNA and 14−15 times slower than that of ds-$(AT)_n$-PNA for large $n$. As described below, the results found here agree best with an incoherent hopping mechanism, in which the charge briefly pauses on the nucleobases.

Because of the slow electron transfer rates observed for the thick films, it is important to consider whether defects can account for the observations. The experimental procedure dictates that electron transfer through defects must involve ferrocene that is tethered to the electrode through a PNA, however. A plausible mechanism would involve diffusive motion of the ferrocene localized on the defect site and/or direct transfer from a ferrocene localized in a defect site. Such a mechanism is similar to that reported by Anne and co-workers[34,35] to describe the electron transfer for SAMs of 20-mer DNA with a ferrocene reporter. They found that the electron transfer had a "soft" distance dependence and modeled their data assuming the diffusive transport of the ferrocene reporter to the electrode surface under the applied field. This mechanism was discounted for the PNA systems studied here for the following reasons. First, a significant difference in the charge transfer rate was found between ss-A-PNA and ss-T-PNA of the same length, even though given their similar length and surface coverage, the diffusive motion of the ferrocene attached to the end of ss-$T_n$ and ss-$A_n$ to the electrode is expected to be similar. Second, our data show that ds-$(AT)_n$-PNA has a higher rate constant than the ss PNAs, even though it is expected to be significantly stiffer than the ss PNAs. Last, the surface coverages of 5 pmol/cm$^2$ of the systems characterized by Anne and collaborators were much lower than that of our SAMs of PNAs, which was ca. 100 pmol/cm$^2$.

An incoherent hopping model in which a hole hops through the nucleobases of the PNA chains can be used to explain the findings, and this model accounts for the dependence of the charge transfer rate on the oxidation potential of the nucleobases. Assuming that the superexchange/tunneling (rate constant $k_{tun}$) and the hopping transport (rate constant $k_{hop}$) act as independent transfer processes, the total rate constant can be written as a sum, namely,

$$k^0 = k_{hop} + k_{tun} = k_{hop} + \nu_{tun} \exp(-\beta(n+1)a) \quad (1)$$

where $\nu_{tun}$ is a preexponential constant and $(n+1)a$ is the distance between the ferrocene and the electrode expressed as a function of the number of nucleobases, or nucleobase pairs, $n$, and of $a$, which is the characteristic length of each of the $n$ monomers or base pairs of the chain. Figure 5 shows a fit of the data for the SAMs of ss PNAs using this equation, under the constraint that they all have the same value of $\nu_{tun}$ (corresponding to the charge transfer rate at $n = 0$, i.e., the cysteine directly connecting the ferrocene to the electrode). The fit to the ss-T-PNA gives the parameters $\beta = 3.07$ per nucleobase and $k_{hop} = 0.0075$ s$^{-1}$; for ss-A-PNA, the fit gives

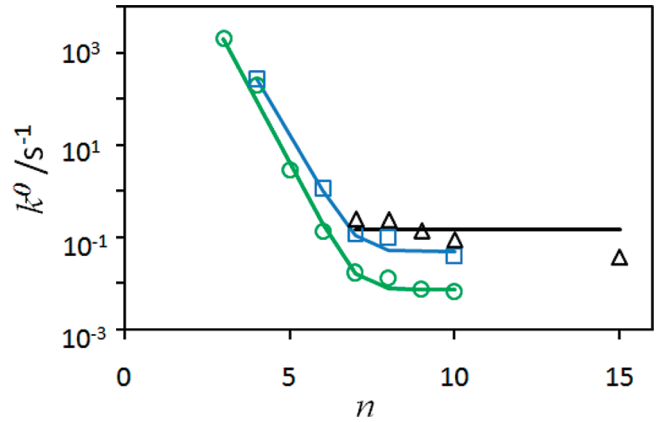


**Figure 5.** Charge transfer rate of PNA molecules plotted as a function of nucleotide number between the Au electrode and the ferrocene. The green circles represent ss-$T_n$-PNA, the blue squares represent ss-$A_n$-PNA, and the black trangles represent ds-$(AT)_n$-PNA. The solid lines represent the best fit by eq 1 (see text for details).

$\beta = 2.80$ per nucleobase and $k_{hop} = 0.05$ s$^{-1}$. At short distances where the tunneling dominates, the distance dependence for ss-$A_n$-PNA is softer than that of the ss-$T_n$-PNA. This observation is consistent with a reduction of the tunneling barrier because of the lower oxidation potential of the A bases.[65]

The most dramatic difference is between $k_{hop}$ for ss-$A_n$-PNA and ss-$T_n$-PNA, with the former ones being 6−7 times larger than the latter. This difference may arise from differences between the rate constant for hole injection onto the bridge, $k_{inj}$. We estimate $k_{inj}$ using a simplified classical Marcus expression[85] (eq 11 of ref 85).

$$k_{inj} = \frac{|V|^2}{\hbar}\rho_m\sqrt{\frac{\pi^3 k_B T}{\lambda}}\exp\left[-\frac{\Delta G_{act}}{k_B T}\right] \quad \text{where}$$

$$\Delta G_{act} = \frac{(\lambda - \varepsilon)^2}{4\lambda} - |V| \quad (2)$$

where $|V|$ is the electronic coupling between a nucleobase and the electrode, $\rho_m$ is an effective density of states in the electrode, $\varepsilon$ is the oxidation energy of the bridge site, and the other symbols have their usual meaning. If we assume that the only difference for the injection rates arises exclusively from the difference in the oxidation energies $\varepsilon$ of the nucleobase, then we find that

$$\frac{k_{inj,A}}{k_{inj,T}} = \exp\left(-\frac{(\lambda - \varepsilon_A)^2 - (\lambda - \varepsilon_T)^2}{4\lambda k_B T}\right)$$

$$= \exp\left(-\frac{(\varepsilon_T - \varepsilon_A)\cdot(2\lambda - \varepsilon_A - \varepsilon_T)}{4\lambda k_B T}\right) \quad (3)$$

If we assume that $\varepsilon_A = 1.27$ eV and $\varepsilon_T = 1.42$ eV,[86] which correspond to the potential shift of A and T relative to the ferrocene/ferrocenium potential, respectively, we obtain a reorganization energy for A and T of $\lambda = 0.81$ eV, a value that is similar to that reported for ferrocene.[66,79]

Figure 5 shows a fit of the rate constant for the duplex PNA data with a fixed, distance independent, rate constant of $k_{hop} = 0.15$ s$^{-1}$. It is evident that the model provides a reasonable treatment of the data for $n$ in the range of 6−10 but does not account for the decrease in rate constant that is observed for $n$

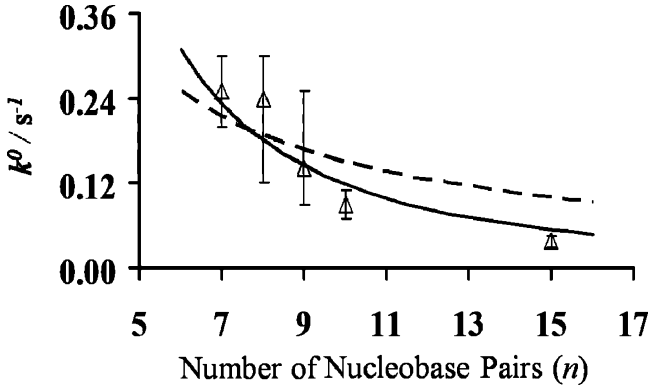


**Figure 6.** Charge transfer rates ($k^0$) of ds-$(AT)_n$-PNA SAMs plotted against the number of nucleobase pairs. The black triangle symbols represent the experimentally determined results, the black line is the fitting to the experimental eq 4, and the dashed line shows the case of $1/n$.

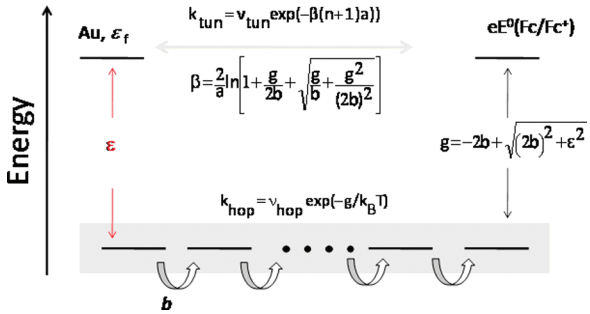


**Figure 7.** Diagram showing a band picture for stacks of Watson−Crick base pairs in PNA. The electronic coupling, $b$, between base pairs leads to the formation of a tight-binding band that has a width of $4b$. $\varepsilon$ represents the energy gap between ferrocene and the base pair levels. $g$ is the energy gap between the redox level and the bottom of the tight-binding conduction band. The energy level for the Fermi level of gold and ferrocene is taken to be the same.

= 15. By treating the hopping transport as diffusive motion, a one-dimensional random walk model can be applied for the charge's motion through the nucleotide chain. Because the chain length is small, we use the solution by Klafter[87,88] for a mean first passage time on a finite chain, which we associate with the characteristic reaction time $1/k^0$.

In this case, the rate constant is given by

$$k^0 \propto \frac{1}{n(n+1)} \tag{4}$$

where $n$ is the number of hopping sites in the bridge that connects the donor and acceptor (see eq 19b of ref 88). Figure 6 plots the charge transfer rates $k^0$ of ds-$(AT)_n$-PNA versus the number of hopping sites ($n$) and a fit of the dependence of $k^0$ on $n$ by eq 4 (solid line). Also shown is a best fit by the function $1/n$ which would be derived from an alternative diffusive model (dotted line), which clearly falls off more softly than the data. The quality of the fit shows that the ds-$(AT)_n$-PNA results are consistent with a one-dimensional diffusion model for charge transfer. A study of PNAs with longer chain lengths and of the dependence of $k^0$ on the temperature is necessary to provide a more rigorous test of this mechanism.

The length of the PNA at which the transition from superexchange/tunneling to hopping transport occurs can be estimated by using a simple tight-binding model (see Figure 7) for charge transfer proposed by Berlin et al.[3] for a similar transition observed in DNA. In this model, the electronic coupling between stacked base pairs leads to the formation of a tight-binding band. The energy gap between the donor/acceptor level and the bottom of the tight-binding conduction band is termed $g$ and can be written as

$$g = -2b + [(2b)^2 + \varepsilon^2]^{1/2} \tag{5}$$

where $b$ is the electronic coupling between adjacent sites on the bridge and $\varepsilon$ is the difference between the energy of the hole on the donor/acceptor and the bridge sites. If the switchover from tunneling to hopping is represented by the condition $k_{tun} = k_{hop}$, then the critical length ($n_{cr}$) of the PNA at which is the switchover occurs is given by

$$n_{cr} = \left[\frac{g}{2k_BT} - \frac{1}{2}\ln\left(\frac{\nu_{hop}}{\nu_{tun}}\right)\right] \times \frac{1}{\ln(1 + x + \sqrt{2x + x^2})} - 1 \tag{6}$$

where $x = g/2b$ and $\nu_i$ are the preexponential factors for the hopping and tunneling rate constants (see ref 3 for details). In the approximation that $\nu_{hop} = \nu_{tun}$, one finds

$$n_{cr} \approx \frac{g}{2k_BT} \times \frac{1}{\ln(1 + x + \sqrt{2x + x^2})} - 1 \tag{7}$$

If $\varepsilon$ is estimated by the oxidation potentials reported for adenine and thymine, namely, 1.27 eV for A and 1.42 eV for T,[86] versus the ferrocene/ferrocenium, then the model can be used to calculate values of $n_{cr}$ for different values of $b$. This calculation gives $n_{cr} = 7$ for T at $b = 0.07$ eV and for A at $b = 0.09$ eV. If the cysteine is considered to be equivalent to an extra nucleobase, then the experimental $n_{cr}$ would be 8; in this case, the model gives a value of $b = 0.1$ eV for T and $b = 0.15$ eV for A. These are plausible values for the internucleobase coupling $b$.[65]

## Conclusions

In this work, ss-$T_n$-PNA, ss-$A_n$-PNA, and ds-$(AT)_n$-PNA oligomers were self-assembled on a gold electrode. The resulting SAMs were characterized by cyclic voltammetry and ellipsometry. Charge transfer through these different PNA SAMs was found to depend on the nucleobase identity and on the number of nucleobases or nucleobase pairs in the PNAs. The ss-$T_n$-PNA had the slowest charge transfer rate. The rate constant for charge transfer in ss-$A_n$-PNA and the ds-$(AT)_n$-PNA was 14−15 times faster, respectively, than that of ss-$T_n$-PNA.

For short chain PNAs, the distance dependence was exponential, which indicates that charge transfer occurs by a superexchange-mediated tunneling mechanism, whereas, for longer chain PNAs, a weaker distance dependence was evident. For the shorter PNA ($n \leq 7$), the tunneling decay constant ($\beta$) was $0.86 \pm 0.04$ Å$^{-1}$ for ss-$T_n$-PNA and $0.76 \pm 0.06$ Å$^{-1}$ for ss-$A_n$-PNA. For longer PNAs, the distance dependence of the rate constant was weak ($\leq 0.1$ Å$^{-1}$). A charge hopping model can be used to explain these data, and it implies that hopping transport be possible for ss PNA SAMs based on thymine nucleobases. While the range of PNA lengths we studied is limited for assessing the mechanism rigorously, the data can be described by a hopping transport mechanism for charge transfer over long distances

in PNA, analogous to the case of DNA. The transition between the superexchange and hopping mechanisms could be rationalized by a tight-binding model[3] that was previously proposed and applied to DNA.

**Acknowledgment.** D.H.W. and C.A. acknowledge support from the U.S. National Science Foundation (CHE 0628169). A.P. thanks Dr. Andrew M. Napper and Dr. Jianjun Wei for useful discussions during this study. We thank Prof. David N. Beratan for useful discussions during this study. C.A. acknowledges support by the Sloan Foundation and the Camille and Henry Dreyfus Foundation. E.W. acknowledges Matthew Kofke for synthesizing octadecylthiosulfate. We acknowledge Helen Wei for synthesizing the Cys-$A_4$-Fc molecule.

**Supporting Information Available:** Data on the melting temperatures of the ds PNAs; mass spectrometry data for the PNAs; details of SAM preparation protocols and control experiments to demonstrate duplex formation, rather than triplex formation; and electrochemical data for the various SAMs reported herein. This material is available free of charge via the Internet at http://pubs.acs.org.

## References and Notes

(1) Arkin, M. R.; Stemp, E. D. A.; Holmlin, R. E.; Barton, J. K.; Hormann, A.; Olson, E. J. C.; Barbara, P. F. *Science* **1996**, *273*, 475–480.
(2) Barnett, R. N.; Cleveland, C. L.; Joy, A.; Landman, U.; Schuster, G. B. *Science* **2001**, *294*, 567–571.
(3) Berlin, Y. A.; Burin, A. L.; Ratner, M. A. *Chem. Phys.* **2002**, *275*, 61–74.
(4) Giese, B.; Wesseley, S. *Angew. Chem., Int. Ed.* **2000**, *39*, 3490–3491.
(5) Conwell, E. M.; Rakhmanova, S. V. *Proc. Natl. Acad. Sci.* **2000**, *97*, 4556–4560.
(6) Giese, B. *Annu. Rev. Biochem.* **2002**, *71*, 51–70.
(7) Giese, B.; Amaudrut, J.; Kohler, A.-K.; Spormann, M.; Wessely, S. *Nature* **2001**, *412*, 318–320.
(8) Henderson, P. T.; Jones, D.; Hampikian, G.; Kan, Y.; Schuster, G. B. *Proc. Natl. Acad. Sci.* **1999**, *96*, 8353–8358.
(9) Jortner, J.; Bixon, M.; Langenbacher, T.; Michel-Beyerle, M. E. *Proc. Natl. Acad. Sci.* **1998**, *95*, 12759.
(10) Jortner, J.; Bixon, M.; Voityuk, A. A.; Rosch, N. *J. Phys. Chem. A* **2002**, *106*, 7599–7606.
(11) Kelley, S. O.; Holmlin, R. E.; Stemp, E. D. A.; Barton, J. K. *J. Am. Chem. Soc.* **1997**, *119*, 9861–9870.
(12) Li, X. Q.; Zhang, H.; Yan, Y. *J. Phys. Chem. A* **2001**, *105*, 9563–9567.
(13) Meggers, E.; Michel-Beyerle, M. E.; Giese, B. *J. Am. Chem. Soc.* **1998**, *120*, 12950–12955.
(14) Murphy, C. J.; Arkin, M. R.; Jenkins, Y.; Ghatlia, N. D.; Bossmann, S. H.; Turro, N. J.; Barton, J. K. *Science* **1993**, *262*, 1025–1029.
(15) Rakhmanova, S. V.; Conwell, E. M. *J. Phys. Chem. B* **2001**, *105*, 2056–2061.
(16) Lewis, F. D.; Wasielewski, M. R. In *Long-Range Charge Transfer in DNA*; Schuster, G. B., Ed.; Top. Curr. Chem. Vol. 236; Springer: New York, 2004.
(17) Schuster, G. B. *Acc. Chem. Res.* **2000**, *33*, 253–260.
(18) Vicic, D. A.; Odom, D. T.; Nunez, M. E.; Gianolio, D. A.; McLaughlin, L. W.; Barton, J. K. *J. Am. Chem. Soc.* **2000**, *122*, 8603–8611.
(19) Berlin, Y. A.; Hutchison, G. R.; Rempala, P.; Ratner, M. A.; Michl, J. *J. Phys. Chem. A* **2003**, *107*, 3970–3980.
(20) Giese, B.; Wessely, S.; Spormann, M.; Lindemann, U.; Meggers, E.; Michel-Beyerle, M. E. *Angew. Chem., Int. Ed.* **1999**, *38*, 996–998.
(21) Lewis, F. D.; Wu, T.; Liu, X.; Letsinger, R. L.; Greenfield, S. R.; Miller, S. E.; Wasielewski, M. R. *J. Am. Chem. Soc.* **2000**, *122*, 2889–2902.
(22) Schwartz, D. K. *Annu. Rev. Phys. Chem.* **2001**, *52*, 107–137.
(23) Ulman, A. *Chem. Rev.* **1996**, *96*, 1533–1554.
(24) Jortner, J.; Ratner, M. A. *Molecular Electronics*; Blackwell: London, 1997.
(25) Giese, B. *Acc. Chem. Res.* **2000**, *33*, 631–636.
(26) Kan, Y.; Schuster, G. B. *J. Am. Chem. Soc.* **1999**, *121*, 10857–10864.
(27) Melvin, T.; Botchway, S.; Parker, A. W.; O'Neill, P. *J. Chem. Soc., Chem. Commun* **1995**, 653.
(28) Drummond, T. G.; Hill, M. G.; Barton, J. K. *J. Am. Chem. Soc.* **2004**, *126*, 15010–15011.
(29) Gorodetsky, A. A.; Buzzeo, M. C.; Barton, J. K. *Bioconjugate Chem.* **2008**, *19*, 2285–2296.
(30) Kelley, S. O.; Boon, E. M.; Barton, J. K. *Angew. Chem., Int. Ed.* **1999**, *38*, 941.
(31) Liu, T.; Barton, J. K. *J. Am. Chem. Soc.* **2005**, *127*, 10160–10161.
(32) Chahma, M.; Lee, J. S.; Kraatz, H.-B. *J. Electroanal. Chem.* **2004**, *567*, 283–287.
(33) Long, Y. T.; Li, C. Z.; Sutherland, T. C.; Chahma, M.; Lee, J. S.; Kraatz, H. B. *J. Am. Chem. Soc.* **2003**, *125*, 8724–8725.
(34) Anne, A.; Demaille, C. *J. Am. Chem. Soc.* **2006**, *128*, 542–557.
(35) Anne, A. s.; Demaille, C. *J. Am. Chem. Soc.* **2008**, *130*, 9812–9823.
(36) Xu, Z.; Li, T. *Nano Lett.* **2004**, *4*, 1105–1108.
(37) Hihath, J.; Xu, B.; Zhang, P.; Tao, N. *Proc. Natl. Acad. Sci.* **2005**, *102*, 16979–16983.
(38) van Zalinge, H.; Schiffrin, D. J.; Bates, A. D.; Haiss, W.; Ulstrup, J.; Nichols, R. J. *ChemPhysChem* **2006**, *7*, 94–98.
(39) Wierzbinski, E.; Arndt, J.; Hammond, W.; Slowinski, K. *Langmuir* **2006**, *22*, 2426–2429.
(40) Nogues, C.; Cohen, S. R.; Daube, S.; Apter, N.; Naaman, R. *J. Phys. Chem. B* **2006**, *110*, 8910–8913.
(41) Nogues, C.; Cohen, S. R.; Daube, S. S.; Naaman, R. *Phys. Chem. Chem. Phys.* **2004**, *6*, 4459–4466.
(42) Guo, X.; Gorodetsky, A. A.; Hone, J.; Barton, J. K.; Nuckolls, C. *Nat. Nano* **2008**, *3*, 163–167.
(43) Degama, A. A. S. *Theor. Chim. Acta.* **1985**, *68*, 159.
(44) Evenson, J. W.; Karplus, M. *Science* **1993**, *262*, 1247–1249.
(45) Gehlen, J. N.; Daizadeh, I.; Stuchebrukhov, A. A.; Marcus, R. A. *Inorg. Chim. Acta* **1996**, *243*, 271–282.
(46) Goldman, C. *Phys. Rev. A* **1991**, *43*, 4500.
(47) Harden, M. M. *J. Chem. Phys.* **1961**, *35*, 508–515.
(48) Joachim, C.; Ratner, M. A. *Nanotechnology* **2004**, *15*, 1065.
(49) Magoga, M.; Joachim, C. *Phys. Rev. B* **1997**, *56*, 4722.
(50) Priyadarshy, S.; Risser, S. M.; Beratan, D. N. *J. Phys. Chem.* **1996**, *100*, 17678–17682.
(51) Ratner, M. A. *J. Phys. Chem.* **1990**, *94*, 4877–4883.
(52) Reimers, J. R.; Hush, N. S. *J. Photochem. Photobiol., A* **1994**, *82*, 31–46.
(53) Remacle, F.; Levine, R. D. *J. Phys. Chem. B* **2001**, *105*, 2153–2162.
(54) Bixon, M.; Giese, B.; Wessely, S.; Langenbacher, T.; Michel-Beyerle, M. E.; Jortner, J. *Proc. Natl. Acad. Sci.* **1999**, *96*, 11713–11716.
(55) Egholm, M.; Buchardt, O.; Christensen, L.; Behrens, C.; Freier, S. M.; Driver, D. A.; Berg, R. H.; Kim, S. K.; Norden, B.; Nielsen, P. E. *Nature* **1993**, *365*, 566–568.
(56) Egholm, M.; Nielsen, P. E.; Buchardt, O.; Berg, R. H. *J. Am. Chem. Soc.* **1992**, *114*, 9677–9678.
(57) Petersson, B.; Nielsen, B. B.; Rasmussen, H.; Larsen, I. K.; Gajhede, M.; Nielsen, P. E.; Kastrup, J. S. *J. Am. Chem. Soc.* **2005**, *127*, 1424–1430.
(58) Rasmussen, H.; Kastrup, J. S.; Nielsen, J. N.; Nielsen, J. M.; Nielsen, P. E. *Nat. Struct. Biol.* **1997**, *4*, 98–101.
(59) Rasmussen, H.; Liljefors, T.; Petersson, B.; Nielsen, P. E.; Kastrup, J. S. *J. Biomol. Struct. Dyn.* **2004**, *21*, 495–502.
(60) He, W.; Hatcher, E.; Balaeff, A.; Beratan, D. N.; Gil, R. R.; Madrid, M.; Achim, C. *J. Am. Chem. Soc.* **2008**, *130*, 13264–13273.
(61) Wittung, P.; Eriksson, M.; Lyng, R.; Nielsen, P. E.; Norden, B. *J. Am. Chem. Soc.* **1995**, *117*, 10167–10173.
(62) Franzini, R. M.; Watson, R. M.; Patra, G. K.; Breece, R. M.; Tierney, D. L.; Hendrich, M. P.; Achim, C. *Inorg. Chem.* **2006**, *45*, 9798–9811.
(63) Popescu, D. L.; Parolin, T. J.; Achim, C. *J. Am. Chem. Soc.* **2003**, *125*, 6354–6355.
(64) Watson, R. M.; Skorik, Y. A.; Patra, G. K.; Achim, C. *J. Am. Chem. Soc.* **2005**, *127*, 14628–14639.
(65) Paul, A.; Bezer, S.; Venkatramani, R.; Kocsis, L.; Wierzbinski, E.; Balaeff, A.; Keinan, S.; Beratan, D. N.; Achim, C.; Waldeck, D. H. *J. Am. Chem. Soc.* **2009**, *131*, 6498–6507.
(66) Paul, A.; Watson, R. M.; Lund, P.; Xing, Y.; Burke, K.; He, Y.; Borguet, E.; Achim, C.; Waldeck, D. H. *J. Phys. Chem. C* **2008**, *112*, 7233–7240.
(67) Azzam, R. M. A.; Bashara, N. M. *Ellipsometry and Polarized Light*; North- Holland Publishing Co: Amsterdam, The Netherlands, 1977.
(68) Tompkins, H. G. *A User's Guide to Ellipsometry*; Academic Press Inc.: Boston, MA, 1993.
(69) Anderson, G. W.; McGregor, A. C. *J. Am. Chem. Soc.* **1957**, *79*, 6180–6183.
(70) McKay, F. C.; Albertson, N. F. *J. Am. Chem. Soc.* **1957**, *79*, 4686–4690.
(71) Nielsen, P. E. *Peptide Nucleic Acids: Protocols and Applications*; Horizon Bioscience: Wymondham, U.K., 2004.
(72) Sawyer, D. T.; Sobkowiak, A.; Roberts, J. L. *Experimental Electrochemistry for Chemists*; Wiley: New York, 1995.
(73) Lee, M. T.; Hsueh, C. C.; Freund, M. S.; Ferguson, G. S. *Langmuir* **2003**, *19*, 5246–5253.
(74) Wittung, P.; Nielsen, P.; Norden, B. *J. Am. Chem. Soc.* **1997**, *119*, 3189.
(75) Haruna, K.-i.; Iida, H.; Tanabe, K.; Nishimoto, S.-i. *Org. Biomol. Chem.* **2008**, *6*, 1613–1617.

(76) Tanabe, K.; Iida, H.; Haruna, K.-i.; Kamei, T.; Okamoto, A.; Nishimoto, S.-i. *J. Am. Chem. Soc.* **2006**, *128*, 692–693.

(77) The length of cysteine, ferrocene, and each PNA base has been calculated by CAChe software. The geometry has been optimized by the PM3 method.

(78) Finklea, H. O. In *Electroanalytical Chemistry*; Bard, A. J., Rubinstein, I., Eds.; Marcel Dekker Inc.: New York, 1996; Vol. 19, p 109.

(79) Napper, A. M.; Liu, H.; Waldeck, D. H. *J. Phys. Chem. B* **2001**, *105*, 7699–7707.

(80) Smalley, J. F.; Feldberg, S. W.; Chidsey, C. E. D.; Linford, M. R.; Newton, M. D.; Liu, Y.-P. *J. Phys. Chem.* **1995**, *99*, 13141–13149.

(81) Carter, M. T.; Rowe, G. K.; Richardson, J. N.; Tender, L. M.; Terrill, R. H.; Murray, R. W. *J. Am. Chem. Soc.* **1995**, *117*, 2896–2899.

(82) Slowinski, K.; Chamberlain, R. V.; Miller, C. J.; Majda, M. *J. Am. Chem. Soc.* **1997**, *119*, 11910–11919.

(83) Sumner, J. J.; Weber, K. S.; Hockett, L. A.; Creager, S. E. *J. Phys. Chem. B* **2000**, *104*, 7449–7454.

(84) Weber, K.; Hockett, L.; Creager, S. *J. Phys. Chem. B* **1997**, *101*, 8286–8291.

(85) Khoshtariya, D. E.; Wei, J.; Liu, H.; Yue, H.; Waldeck, D. H. *J. Am. Chem. Soc.* **2003**, *125*, 7704–7714.

(86) Seidel, C. A. M.; Schulz, A.; Sauer, M. H. M. *J. Phys. Chem.* **1996**, *100*, 5541–5553.

(87) Bar-Haim, A.; Klafter, J. *J. Chem. Phys.* **1998**, *109*, 5187–5193.

(88) Wang, X.; Nau, W. M. *ChemPhysChem* **2001**, *2*, 761–766.

JP906910H